3D microstructural study of selachimorph enameloid evolution

C. Fellah, T. Douillard, E. Maire, S. Meille, B. Reynard, G. Cuny

HAL Id: hal-03034289

https://hal-univ-lyon1.archives-ouvertes.fr/hal-03034289

Submitted on 24 Feb 2021

3D microstructural study of selachimorph enameloid evolution

C. Fellah [a,*], T. Douillard [b], E. Maire [b], S. Meille [b], B. Reynard [a], G. Cuny [c]

[a] *Université de Lyon, ENS Lyon, Université Lyon 1, CNRS, LGL-TPE, F-69007 Lyon, France*
[b] *Université de Lyon, INSA-Lyon, UMR CNRS 5510 MATEIS, Villeurbanne Cedex, France*
[c] *Univ Lyon, Université Claude Bernard Lyon 1, CNRS, ENTPE, UMR5023 LEHNA, F-69622, Villeurbanne, France*

Enameloid, the hyper-mineralized tissue covering shark teeth is a complex structure resulting from both ameloblast and odontoblast activity. The way these two types of cells interact to set up this tissue is not fully understood and results in the formation of subunits in the enameloid: the Single Crystallite Enameloid (SCE) and the Bundled Crystallite Enameloid (BCE). Using the Focused Ion Beam Nanotomography (FIB-nt), 3D images were produced to assess the relationship between the SCE and BCE of one fossil and one recent neoselachian shark teeth. 3D analysis of crystallite bundles reveals a strong connection between the crystallites forming the SCE and those forming the bundles of the Radial Bundle Enameloid (RBE), a component of the BCE, although it has been suggested that SCE and BCE have a different origin: epithelial for the SCE and mesenchymal for the BCE. Another significant result of the use of FIB-nt is the visualization of frequent branching among the radial bundles forming the RBE, including horizontal link between adjacent bundles. FIB-nt demonstrates therefore a strong potential to decipher the complex evolution of hyper-mineralised tissue in shark teeth, and, therefore, to better understand the evolution of tooth structure among basal Gnathostomes.

1. Introduction

Elasmobranchs possess many teeth, frequently replaced, which makes this material quite easy to find and study. Their hard structure allows them to be fossilized more easily than their cartilaginous skeletons, which remain rare in the fossil record (Cappetta, 2012).

Enameloid, the hyper-mineralized tissue covering most chondrichthyan teeth, has a complex microstructure. This biomaterial is made from a biological fluorapatite composed of elongated mineral crystallites and a collagen-rich extracellular matrix (LeGeros and Suga, 1980; Dahm and Risnes, 1999; Daculsi and Kerebel, 1980). Its mineralization precedes that of the dentine, whereas it is the reverse among tetrapod teeth, which display enamel instead of enameloid. Enamel is produced exclusively by ameloblast cells of epithelial origin, whereas the dentine is the results of odontoblast cells activity, which are of mesenchymal origin. On the other hand, enameloid is attributed to both ameloblasts and odontoblasts (Francillon-Vieillot et al., 1990; Gillis and Donoghue, 2007), with a contribution of each of these cells that remains debated. The main component of shark enameloid is fluorapatite ($Ca_5(PO_4)_3F$), a fluorine-rich calcium phosphate (Baddiel and Berry, 1966; Bowen, 1965; Beevers and McIntyre, 1946). The high fluor content lowers the dissolution potential of this apatite and improves the hardness of the material with respect to hydroxyapatite, with higher stiffness and elastic modulus (Gardner et al., 1992; Yoon and Newnham, août, 1969).

Neoselachian teeth exhibit a complex enameloid made of two units (Fig. 1) (Enault et al., 2015; Cuny et al., 2018; CUNY et al., 2001). The external unit, named SCE (Single Crystallite Enameloid), is composed of distinct crystallites with a random orientation. Each microcrystal has a 1–2 µm length and a width not exceeding 0.2 µm. The inner unit, named BCE (Bundled Crystallite Enameloid), has crystallites aggregating into bundles, whose diameter is comprised between 5 and 10 µm. Three components are defined according to the organization of the bundles:

- The PBE (Parallel-Bundled Enameloid) where the bundles are oriented parallel to each other and to the surface of the tooth;
- The RBE (Radial-Bundled Enameloid) where the bundles are oriented perpendicular to the surface of the tooth;
- The TBE (Tangled-Bundled Enameloid) where the bundles intermingle with each other without preferential orientation.

* Corresponding author at: Laboratoire de Géologie de Lyon: Terre, Planètes, Environnement, UMR CNRS 5276 (CNRS, ENS, Université Lyon1), Ecole Normale Supérieure de Lyon, 9 rue du Vercors, 69364 Lyon cedex 07, France.
E-mail address: clementine.fellah@ens-lyon.fr (C. Fellah).
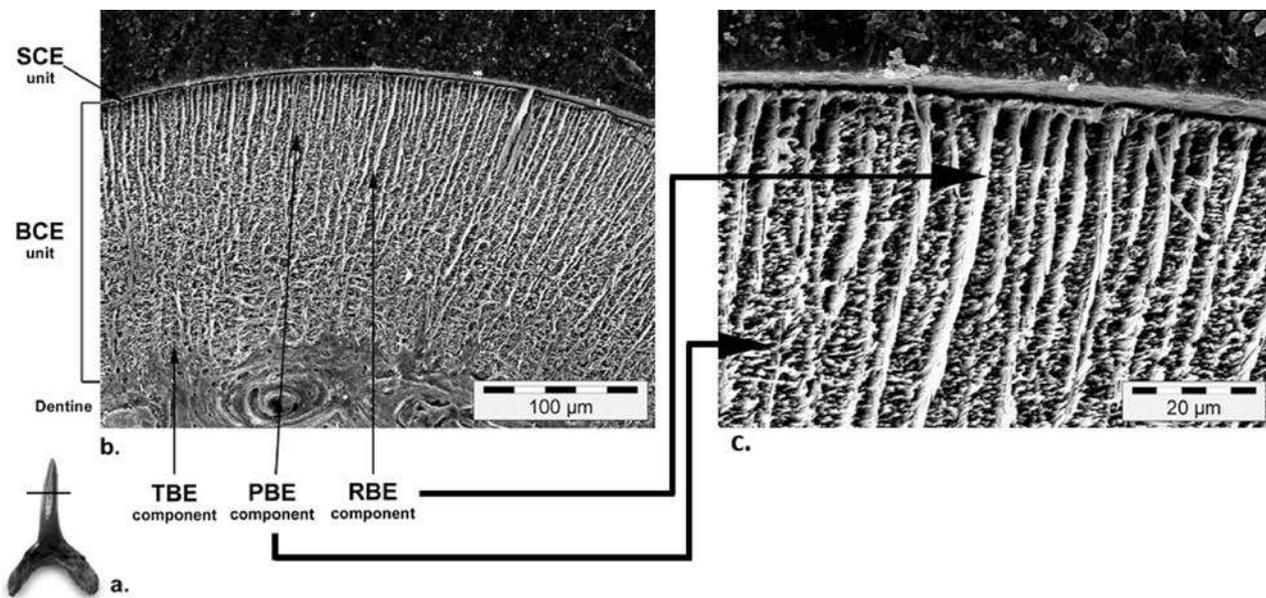
Fig. 1. Tooth of *Anomotodon novus* from the Ypresian Nanjemoy Formation of Virginia in labial view. Photo by Sten Lennart Jakobsen. The horizontal bar visualizes the transverse section plan (a.). Transverse section of the enameloid of the tooth visualizing the arrangement of the microstructure of the tissue in two units: Single Crystallie Enameloid (SCE), too thin to be properly seen, and Bundled Crystallite Enameloid (BCE). The latter is made of three units: Parallel-Bundled Enameloid (PBE), the bundles of which are oriented perpendicular to the plan of the image, Radial-Bundled Enameloid (RBE) and Tangled-Bundled Enameloid (TBE) (b.). Enlargement of the upper part of the enameloid to better visualize the PBE and RBE (c.).

Note that, to reveal ultrastructure, the transverse section was etched 5 s with 4% hydrochloric acid (HCl). The etching produces selective dissolution between the mineralized parts of the tooth and the recrystallized matrix following the fossilization process.

Enameloid microstructure can be studied by scanning electron microscopy (SEM) using two main methods (G.-G. F and G. Aj., 1991; Seow and Amaratunge, 1998; Marshall et al., 1975). The first is to observe the enameloid in longitudinal or transversal section after mechanical cutting of the tooth, followed by polishing and short acid etching of the section. The second is based on successive acid etching in order to map the distribution of the different microstructures over the entire tooth surface. However, these methods permit only a study in two dimensions.

The FIB-SEM tomography (FIB-nt) is widely used in Materials and Life Sciences (Giannuzzi and University, 2004; Munroe, 2009; Drobne et al., 2013) but still rarely in Earth Sciences and Palaeontology. This powerful technique has already been used to study the three-dimensional structure of dentin (Sezen et al., 2014; EARL et al., 2010; Vennat et al., 2002) and makes it possible to build volumes with a nanometric resolution. The principle of the FIB-nt is based on stacking 2D images, obtained by alternate serial FIB milling and SEM imaging, to reconstruct the microstructure in three dimensions. The volume reconstructed by interpolation between two images can typically reach thousands of μm^3. Unlike X-ray tomography, inconvenience of FIB-nt is its destructive nature. However, ion milling does not induce selective dissolution as acid etching does.

In this study, the enameloid of an extant carcharhiniform shark was compared to that of an extinct lamniform shark. Although these two sharks are not closely related, previous studies (Reif, 1974) have demonstrated a similar microstructure of their enameloid, allowing to compare and better understand differences due to fossilization processes. These teeth were observed in cross section by conventional scanning electron microscopy in order to obtain initial microstructural information. The FIB-nt technique was applied to obtain 3D reconstructions of the enameloid where SCE meets BCE for both sharks. Consequences for dental microstructure of elasmobranchs hypermineralized tissue are discussed.

2. Experimental procedure

2.1. Materials

Two teeth of modern carcharhiniform sharks, belonging to the genus *Carcharhinus,* were bought at the Digue market in Antananarivo by one of us (GC) on April 23rd 1996. Their origin was indicated as coming from Toliara, a coastal city situated in the Southwest part of Madagascar. The teeth being isolated, identification at species level was not possible.

The fossil sample, provided by J. Martin, can be referred to *Carcharias* sp., a lamniform from the Late Cretaceous (Campanian unit), collected at *Cap de Naze*, Senegal (Cuny et al., 2012). The animal tissues used in this article were provided and used with permission and following the ethical guidelines of the University Claude Bernard-Lyon1.

2.2. Scanning electron microscopy (SEM)

Classic preparation methods allow observation of the different microstructures of teeth in section or from the surface but is time-consuming (Gillis and Donoghue, 2007; Enault et al., 2015). It is also difficult to evaluate how acid etching alters the global enameloid microstructure. To overcome these problems, the broad ion beam (BIB) milling technique was used to prepare polished surfaces of shark teeth by argon ion bombardment.

The BIB polished sections were prepared as transverse cross-section of the shark teeth apex. Teeth samples were glued with a silver paint onto a titanium blade. The BIB (Gatan Ilion II System) polished cross sections (around 20000 μm^2), using an argon beam with an energy set to 6KV for 3 h of milling under vacuum (5.10^{-5} Pa).

BIB-polished samples were observed using a FIB-SEM workstation (NVision 40; Carl Zeiss Microscopy) coupling a SIINT zeta ionic column (Seiko Instruments Inc. NanoTechnology, Japan) with a Zeiss Gemini I electronic column. These observations were made in high vacuum, operated at 1 kV with a back-scattered electron (BSE) detector, without coating. SEM images have been processed by ImageJ (Collins, 2007), an
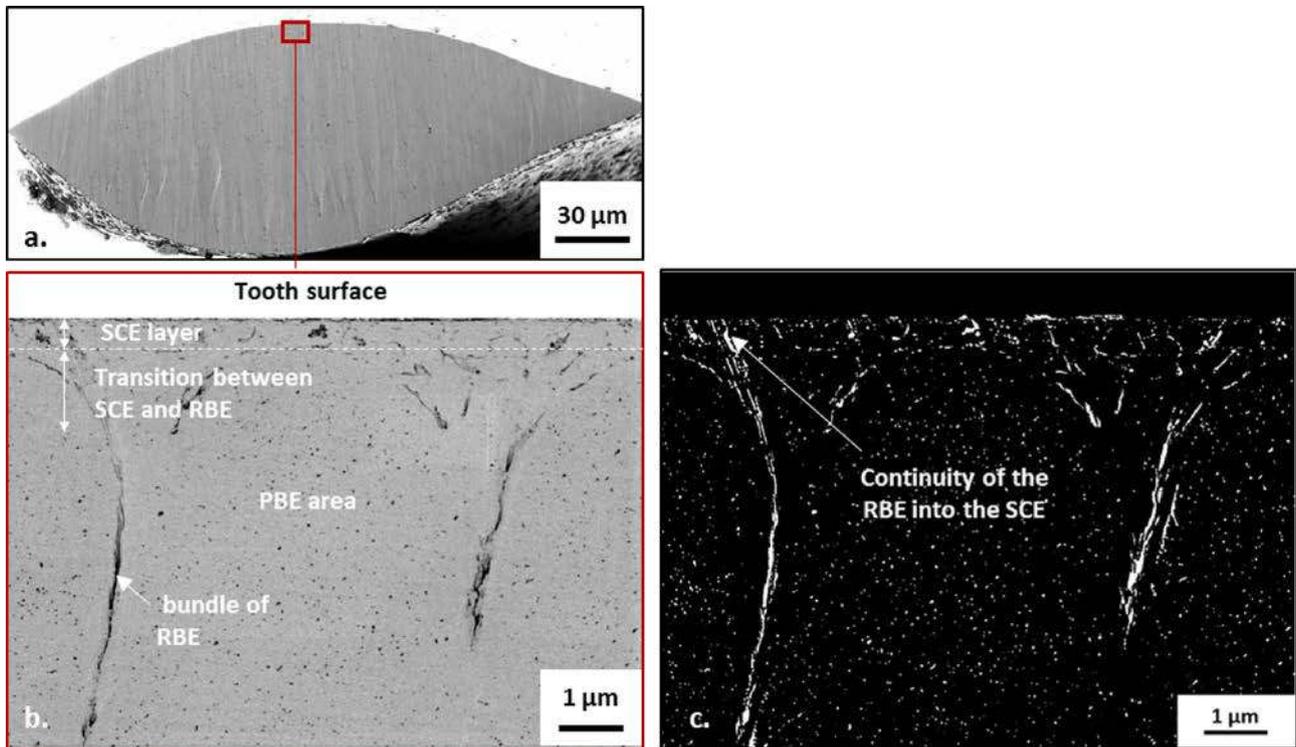
Fig. 2. Cross-section of a tooth of a modern *Carcharhinus* after BIB preparation: SEM analysis and image processing. (a.) Overview of the whole cross-section and zoom near the surface in (b.) – (c.) Binary image from thresholding of (b.): Going to the surface, the bundles of the RBE "open up" like flowers and lose their tightly packed, parallel to each other organization. A continuity between crystallites of the RBE and SCE is observed.

open-source image processing package, to obtain more microstructural information. The VSNR algorithm (Fehrenbach et al., 2012) was used to remove stationary noise and to limit the curtaining effect due to ion abrasion during sample preparation. Subsequently, a thresholding method (Xu et al., 2011; Zhang and Hu, 2008) was chosen to create binary images, with elements of interest in white pixels clusters and the background in black, from grayscale images. This method iterates over all possible threshold values and calculates the spread of the pixel levels each side of the threshold to find the optimum.

2.3. FIB-SEM tomography

For FIB operation, teeth samples were remounted with a silver paint onto an aluminium stub and coated with a gold layer of about 50 nm by sputtering (EM SCD500, Leica Microsystems GmbH, Germany) to prevent electrostatic charging.

The FIB-SEM serial sectioning experiments were performed with the FIB-SEM workstation (NVision 40; Carl Zeiss Microscopy) used to observe BIB-polished samples. The Atlas 3D software (FIBICS Incorporated, Ottawa, CA), an external scanning system, was used to drive the device.

First, a carbon coating (20×20 μm^2) was deposited with the *insitu* gas injection system to define a target area and to protect the surface from ion beam damage. A pattern generated by milling the carbon coating is used for refocusing during acquisition and as markers for image alignment during 3D reconstruction (Mainjot et al., 2013). These marks were enhanced with tungsten deposition and were protected with a last carbon coating. Prior to serial milling and imaging, a coarse trench was milled around the region of interest to a depth of 30 μm.

2D imaging of each slide was conducted using backscattered electrons with the so-called Energy and angle selective BSE detector (EsB) and secondary electrons with the Secondary Electrons Secondary Ions detector (SESI). The FIB-nt experiments were performed at 1.5 kV with a grid potential set to 800 V (EsB). For serial sectioning, FIB milling

parameters were adjusted to 30 kV and 1.5nA. These experimental conditions were chosen to fit a cubic voxel size of $20 \times 20 \times 20$ nm^3. Each stack contains 350 to 700 slices with a target slice thickness of 20 nm.

After raw data acquisition, the image processing was performed in several stages using the ImageJ software. The slices were aligned to correct spatial drifts in the x- and y-directions, due to mechanical and environmental disturbances such as electrostatic charging, with the plugin MultiStackReg. The image alignment results in a loss of voxels at the edges of the volume because of the slice shifting. These useless data were removed to obtain a smooth parallelepiped. The plugin bleach correction was used to remove illumination defect of the stack, such as the shadowing effect. The VSNR algorithm was applied to reduce noise related to curtaining effect on each slice. The treatment involved also other image filters to improve contrast and brightness. After segmentation and thresholding operations, the stack of 2D slices was transformed into a voxel-based data volume where microstructural characteristics were highlighted by labelling. The overall procedure is illustrated in detail in Cougot et al. (Cougot et al., 2018a, 2018b). Other computational operations were directly performed in this volume. Among them, we perfomed Z-projections of the whole stacks of 2D SEM images to visualize 3D data in 2D. We use a method consisting in adding intensity along the *z* axis for each *pixel* position. This means superimposing several images in one and having a global view of the details within a volume along an axis.

3. Results

3.1. 2D enameloid microstructural organization

In the extant *Carcharhinus* tooth, contrast is observed between the fluorapatite crystallites and organic matter. The sample preparation method did not reveal the enameloid crystallite clusters but the microstructural pattern of the protein matrix between the crystallites or
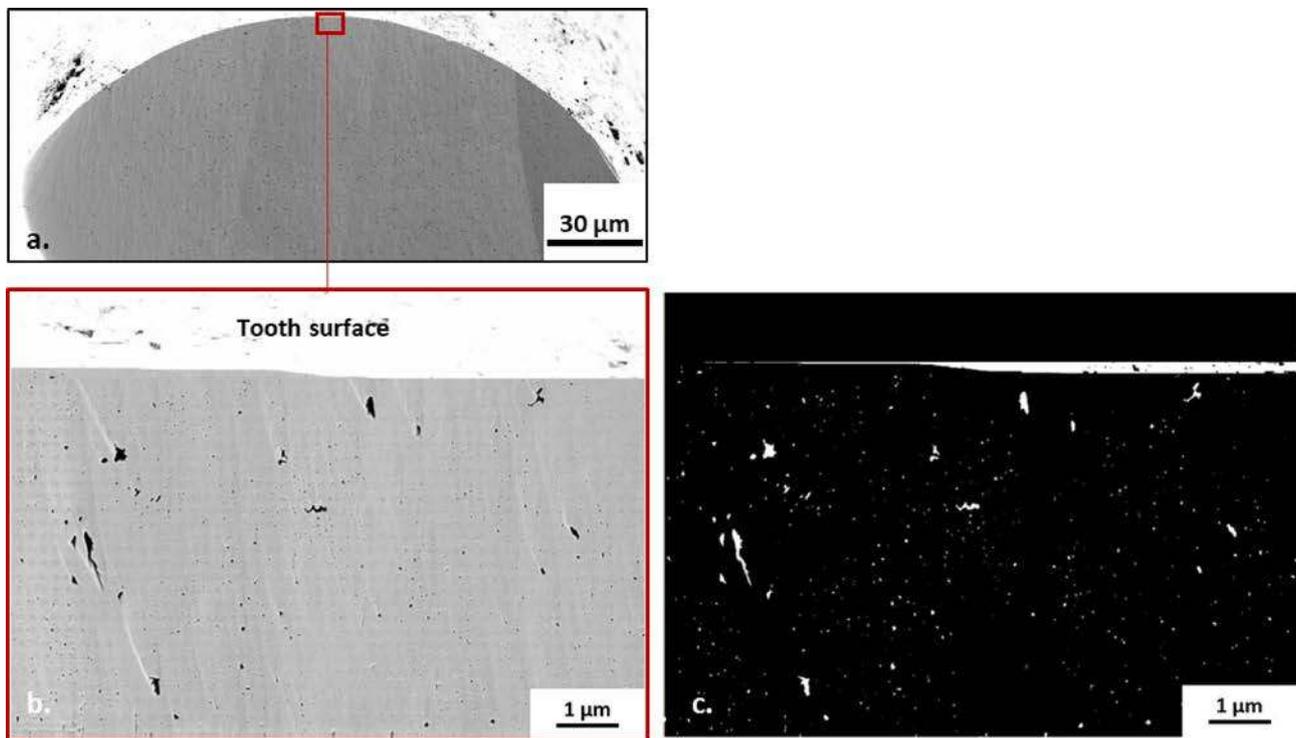
Fig. 3. Cross-section of a tooth of a fossil *Carcharias* after BIB preparation: SEM analysis and image processing. (a.) Overview of the whole cross-section and zoom near the surface in (b.) – (c.) Binary image from thresholding of (b.): Enameloid components of the fossil shark teeth are not highlighted neither by 2D SEM imaging nor by subsequent segmentation.

bundles of the sample (Fig. 2a). In the BCE unit, the crystallite bundles parallel to the tooth surface are separated from each other by protein matrix, represented by the white dots on the segmented image (Fig. 2b). The network of radial bundles surrounded by the protein matrix is also observed. In the upper 2.5 μm of the enameloid (SCE), the bundles of the RBE "open up" like flowers and their crystallites lose their tightly packed, parallel to each other organization. A continuity between crystallites of the RBE and SCE is observed (Fig. 2c). The interest of BIB has been to ensure the conservation of the entire enameloid with respect to etching that may have removed the upper worn and disorganised SCE.

In the fossil *Carcharias* sample, the three distinct layers usually observed in modern shark teeth (selachimorphs) were not visible as the sample was not acid etched (Fig. 3). The BIB section of the apex did not make it possible to differentiate the different units and microstructural characteristics of the enameloid due to extensive mineralization of the sample after fossilization.

3.2. 3D microstructural organization of extant Carcharhinus enameloid

In the modern *Carcharhinus* enameloid, a volume of $18.3 \times 17.7 \times 6.9$ μm^3 volume was acquired in 12 h and a voxel size of $20 \times 20 \times 20$ nm (Fig. 4a). The Z-projection of the 3D representation confirms the results obtained by the 2D microstructural analysis (§ 3.1). The Fig. 4b highlights the continuity of the crystallites network between RBE and SCE units but also the presence of transverse interconnections between radial bundles in the RBE. The microstructural characteristics of *Carcharinus* enameloid were identified in different colours by labelling operations performed in 3D space (Fig. 4c, 4b and 4e). The enameloid structure shows a SCE unit of ~ 1 μm, the upper part is in brown. The spaces between the crystallites oriented parallel to each other and to the surface of the tooth, forming the PBE component of the BCE unit, are shown in cyan. In orange, radial crystallites of the RBE create a periodic lattice and expand to the outermost surface of the tooth. The orthogonal projection just under the surface (Fig. 4f) confirm clearly the network continuity of anastomosed radial bundles in the SCE.

### 3.3. 3D microstructural organization of fossil Carcharias enameloid

A $19.0 \times 19.1 \times 14.0$ μm^3 (5080.6 μm^3) volume was reconstructed following FIB-SEM tomography experiment on the *Carcharias* sp. tooth during about 20 h- acquisition time with a similar voxel size (Fig. 5a).

Contrary to the classical SEM images (§ 3.1), SEM images obtained with the FIB-nt routine displays a faint multi-layered structure. In order to enhance this structure, the Z-projection was performed by summing the slices of the 3D volume acquired with SESI and EsB detectors (Fig. 5b). Although the protein matrix has largely decayed in the fossil, the matrix-bundle contrast in the inner part was observed as well as in the upper layer with a 2.5-μm thickness, and displays a similar structure with SCE and BCE as that observed in the extant shark tooth. It was imaged using the same colour code as in Fig. 6 (Fig. 5c, 5d and 5e); RBE is in orange, PBE in cyan and top SCE boundaries in brown. Several cracks in violet (high contrast level on the BSE acquisition) go through the whole sample and are due to geological processes.

The SCE layer (Fig. 5f) is thicker in the fossil *Carcharhias* teeth than in extant *Carcharinus* teeth. The difference in SCE thickness between the two samples may have a phylogenetic origin, since the teeth belong to different genera, rather than a diagenetic one. In the volume, radial bundles have many interconnected ramifications with the SCE.

4. Discussion

FIB-nt allowed obtaining details of the microstructural organization of the enameloid of selachimorphs never observed before. It shows that the structure of the two studied teeth are similar to each other even if the samples belong to two different orders (Carcharhiniformes and Lamniformes) separated by more than 70 million years. This suggests that the structures observed are widely distributed among at least galeomorph sharks and stable through time. The SCE unit appears composed of a wide network of entangled crystallites. This crystallite network is observed to originate from the bundles forming the RBE at the SCE/BCE interface, although it has been suggested that the SCE of selachimorph
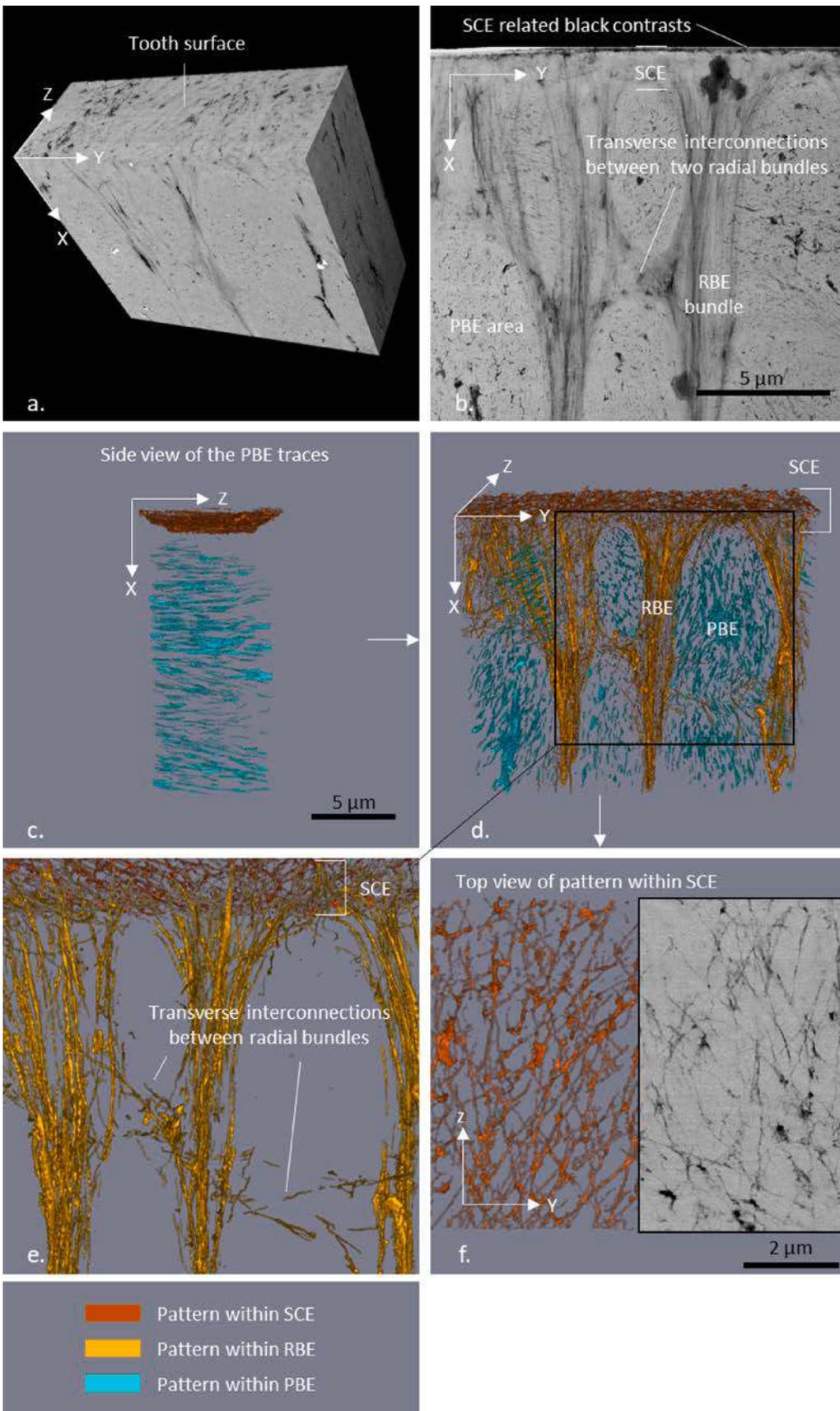
Fig. 4. 3D FIB/SEM for Modern *Carcharhinus* enameloid. (a.) Volume after registration of 2D SEM images (18.3 × 17.7 × 6.9 μm^3, Voxel size: 20 × 20 × 20 nm^3) - (b.) Production of a composite 2D image from a Sum -projection in the *z* direction (i.e. along the axis perpendicular to image plane) of all the slices in the stack. This method allows to clearly make out the enameloid components and highlight transverse few connections between RBE - (c.) Orthogonal view along the Y-axis (after segmentation) of the PBE traces (in cyan) and of the superficial part of the SCE (in brown) – The RBE component is not displayed here. For PBE, the bundles are oriented parallel to each other and to the surface of the tooth - (d.) 3D reconstruction after segmentation of the enameloid components in the volume using contrast thresholding and shape filtering. RBE is in orange, PBE in cyan and top SCE in brown. Note the continuity of the RBE bundles into the SCE area zoomed in (e.) as interconnection between RBE bundles - (f.) Extracted from the volume, left: top view i.e. (along the X-axis) of the segmented black contrasts within SCE (flagged in b.) – right: reconstructed 2D SEM image of the same area in the ZY plane.
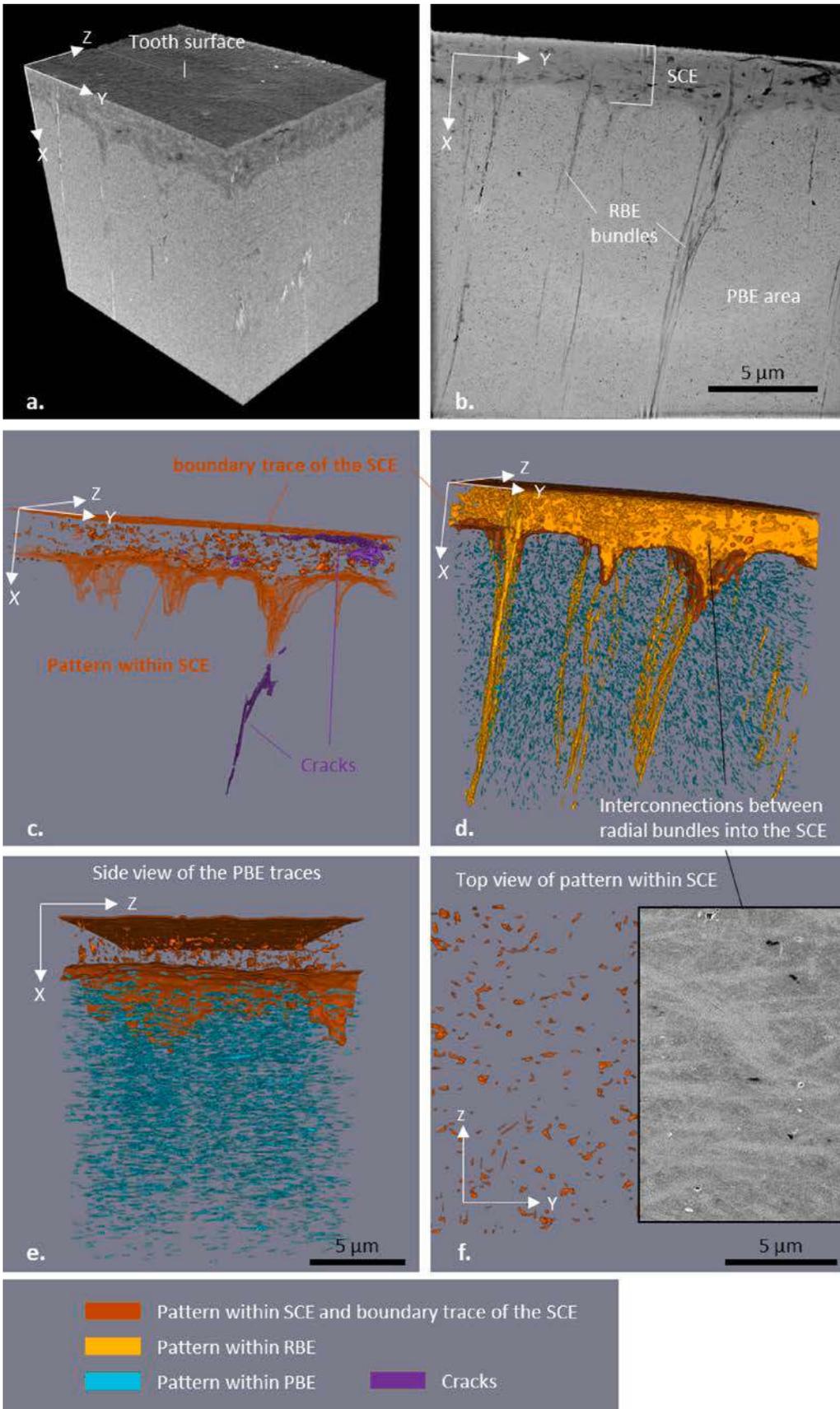
Fig. 5. 3D FIB/SEM for fossil *Carcharias* enameloid (a.) Volume after registration of 2D SEM images (19.0 × 19.1 × 14.0 μm³, Voxel size: 20 × 20 × 20 nm³) - (b.) Z-projection to the whole stack of 2D SEM images. The enameloid components are highlighted. The thickness of the SCE is around 2,5μm – (c.) Reconstructed view of both boundary of the SCE and specific contrasts inside (in brown). Several cracks (in violet) go through the whole sample and may be due to geological processes. (d.) 3D reconstruction after segmentation of the enameloid components in the volume using contrast thresholding and shape filtering. RBE is in orange, PBE in cyan and top SCE boundaries in brown. RBE spreads to a great extent into SCE – (e.) Orthogonal view along the Y axis (after segmentation) of the PBE traces (in cyan) and of specific patterns of the SCE (in brown) – The RBE component is not displayed here. PBE keeps contiguous to SCE – (f.) Extracted from the volume, left: top view i.e. (along the X axis) of segmented contrasts within SCE (in brown) – right: reconstructed 2D SEM image of the same area in the ZY plane with entangled contrasts.

sharks could be of epithelial origin whereas the BCE was of mesenchymal origin (Cuny and Risnes, 2005). Guinot and Cappetta (Guinot and Cappetta, 2011) illustrated also a very similar organization in the enameloid of teeth of Hexanchiformes and of *Synechodus*, although we did not observe the two-layered SCE they describe (Guinot and Cappetta, 2011). On the contrary, our results suggest that the whole of the SCE derived from the RBE. The use of FIB methods on Hexanchiformes teeth would certainly allow demonstrating whether the whole of the SCE derives from the RBE in these sharks as well and whether the presence of a double-layered SCE is an artefact due to the limitations of 2D studies. It was recently suggested (Delaunois et al., 2020.), based on a study of the acrodin of serrasalmid bony fishes, that the cuticle of the acrodin is homologous with the SCE of selachimorph sharks, that the inner enameloid, including the cuticle and dense bundled enameloid, is of epithelial origin while the inner enameloid is of mesenchymal origin. Such a hypothesis would explain the close relationships between SCE and RBE observed here.

Another significant result of the use of SEM-FIB is the clear visualization of frequent branching among the radial bundles forming the RBE, including horizontal link between adjacent bundles. The latter structure was also figured by Guinot and Cappetta (2001) in hexanchiform teeth. Bundles of the RBE are therefore more interconnected than hitherto suspected. This could represent a synapomorphy for the selachimorphs, although more studies will be needed to confirm this hypothesis. Characterizing selachimorphs from their enameloid microstructure has been indeed more problematic since the presence of a PBE in cladodont sharks has been demonstrated by Guinot et al. (2013).

5. Conclusion

The 3D reconstruction of enameloid brings a new perspective on this tissue microstructure among selachimorphs. It is first observed that crystallites of the SCE is closely interconnected with those of the RBE although these two components have been proposed to be of different origin. Hence, a more clear-cut boundary between them was hitherto considered. This observation holds for both modern and fossil sharks. Secondly, a 3D reconstruction of the superficial part of the enameloid allows visualizing in detail the branching pattern of the bundles forming the RBE, which is more intricate than hitherto thought. This has the potential to offer a synapomorphy to characterize selachimorph enameloid although more studies will be needed. It should also be investigated whether this branching pattern is also present in the deeper part of the tissue. 3D visualization of enameloid microstructure is therefore a powerful tool for our understanding of the evolutionary pattern of selachimorph enameloid and of the earliest biomineralization processes.

CRediT authorship contribution statement

C. Fellah: Conceptualization, Investigation, Writing - original draft, Writing - review & editing. **T. Douillard:** Methodology, Investigation, Writing - review & editing. **E. Maire:** Writing - review & editing, Supervision. **S. Meille:** Supervision. **B. Reynard:** Writing - original draft, Supervision. **G. Cuny:** Conceptualization, Resources, Writing - original draft, Writing - review & editing, Supervision, Project administration, Funding acquisition.

Declaration of Competing Interest

The authors declare that they have no known competing financial interests or personal relationships that could have appeared to influence the work reported in this paper.

References

Baddiel, C.B., Berry, E.E., 1966.. Spectra structure correlations in hydroxy and fluorapatite. Spectrochim. Acta 22 (8), 1407–1416.

Beevers, C.A., McIntyre, D.B., 1946. The atomic structure of fluor-apatite and its relation to that of tooth and bone material. (With Plates XVI-XVIII.). Mineral. Mag. j. Mineral. Soc. 27 (194), 254–257.

Bowen, R.L., 1965. Adhesive Bonding of Various Materials to Hard Tooth Tissues. IV. Bonding to Dentin, Enamel, and Fluorapatite Improved by the Use of a Surface-active Comonomer. J. Dent. Res. 44 (5), 906–911.

Cappetta, H.A., 2012. Chondrichthyes : Mesozoic and Cenozoic Elasmobranchii : teeth. F. Pfeil.

Collins, Tony J., 2007. ImageJ for microscopy. Biotechniques 43 (1S), S25–S30.

Cougot, Nancie, Douillard, Thierry, Dalmas, Florent, Pradelle, Nelly, Gauthier, Rémy, Sanon, Clarisse, Grosgogeat, Brigitte, Colon, Pierre, Chevalier, Jérome, 2018ab. Towards quantitative analysis of enamel erosion by focused ion beam tomography. Dent. Mater. 34 (11), e289–e300.

Cuny, G., Guinot, G., Enault, S., 2018. Evolution of Dental Tissues and Paleobiology in Selachians. Elsevier.

Cuny, Gilles, Martin, Jeremy E., Sarr, Raphaël, 2012. A neoselachian shark fauna from the Late Cretaceous of Senegal. Cretac. Res. 34, 107–115.

Cuny, G., Risnes, S., 2005. The enameloid microstructure of the teeth of Synechodontiform sharks (Chondrichthyes: Neoselachii). Pal. Arch. 3 (2), 8–19.

Cuny, G., Rieppel, O., Sander, P.M., 2001. The shark fauna from the Middle Triassic (Anisian) of North-Western Nevada. Zool. J. Linn. Soc. 133 (3), 285–301.

Daculsi, G., Kerebel, L.M., 1980. Ultrastructural study and comparative analysis of fluoride content of enameloid in sea-water and fresh-water sharks. Arch. Oral Biol. 25 (3), 145–151.

Dahm, S., Risnes, S., 1999. A Comparative Infrared Spectroscopic Study of Hydroxide and Carbonate Absorption Bands in Spectra of Shark Enameloid, Shark Dentin, and a Geological Apatite. Calcif. Tissue Int. 65 (6), 459–465.

Delaunois, Y., Huby, A., Malherbe, C., Eppe, G., Parmentier, É., Compère, P., 2020.. Microstructural and compositional variation in pacu and piranha teeth related to diet specialization (Teleostei: Serrasalmidae). J. Struct. Biol. 210 (3), 107509.

Drobne, D. 2012. 3D Imaging of Cells and Tissues by Focused Ion Beam/Scanning Electron Microscopy (FIB/SEM), in: A. A. Sousa et M. J. Kruhlak, (Éds.) Nanoimaging: Methods and Protocols, Totowa, NJ, Humana Press, pp. 275-292.

Earl, J.S., Leary, R.K., Perrin, J.S., Brydson, R., Harrington, J.P., Markowitz, K., Milne, S. J., 2010. Characterization of dentine structure in three dimensions using FIB-SEM. J. Microsc. 240 (1), 1–5.

Enault, S., Guinot, G., Koot, M.B., Cuny, G., 2015. Chondrichthyan tooth enameloid: past, present, and future: Chondrichthyan Tooth Enameloid. Zool. J. Linn. Soc. 174 (3), 549–570.

Fehrenbach, J., Weiss, P., Lorenzo, C., 2012. Variational Algorithms to Remove Stationary Noise: Applications to Microscopy Imaging. IEEE Trans. Image Process. 21 (10), 4420–4430.

Francillon-Vieillot, H., de Buffrénil, V., Castanet, J., Géraudie, J., Meunier, F.J., Sire, J.Y., Zylberberg, L., de Ricqlès, A., 1990. Microstructure and mineralization of vertebrate skeletal tissues. In: Carter, J.G. (Ed.), Skeletal biomineralization: patterns, processes and evolutionary trends. Van Nostrand Reinhold, New York, NY, pp. 471–530.

G.-G. F and G. Aj, juin 1991. Effect of etching times and mechanical pretreatment on the enamel of primary teeth: an SEM study, Am. J. Dent., vol. 4, n 3, p. 115-118.

Gardner, T.N., Elliott, J.C., Sklar, Z., Briggs, G.A.D., 1992. Acoustic microscope study of the elastic properties of fluorapatite and hydroxyapatite, tooth enamel and bone. J. Biomech. 25 (11), 1265–1277.

Giannuzzi L. A., University N. C. S. 2004. Introduction to Focused Ion Beams: Instrumentation, Theory, Techniques and Practice. Springer Science & Business Media.

Gillis, J.A., Donoghue, P.C.J., 2007. The homology and phylogeny of chondrichthyan tooth enameloid. J. Morphol. 268 (1), 33–49.

Guinot, Guillaume, Adnet, Sylvain, Cavin, Lionel, Cappetta, Henri, 2013. Cretaceous stem chondrichthyans survived the end-Permian mass extinction. Nat. Commun. 4 (1).

Guinot, Guillaume, Cappetta, Henri, 2011. Enameloid microstructure of some Cretaceous Hexanchiformes and Synechodontiformes (Chondrichthyes, Neoselachii): New structures and systematic implications. Microsc. Res. Tech. 74 (2), 196–205.

LeGeros, R.Z., Suga, S., 1980. Crystallographic nature of fluoride in enameloids of fish. Calcif. Tissue Int. 32 (1), 169–174.

Mainjot, Amélie K., Douillard, Thierry, Gremillard, Laurent, Sadoun, Michaël J., Chevalier, Jérôme, 2013. 3D-Characterization of the veneer–zirconia interface using FIB nano-tomography. Dent. Mater. 29 (2), 157–165.

Marshall, G.W., Olson, L.M., Lee, C.V., 1975. SEM Investigation of the Variability of Enamel Surfaces After Simulated Clinical Acid Etching for Pit and Fissure Sealants. J. Dent. Res. 54 (6), 1222–1231.

Munroe, P.R., 2009. The application of focused ion beam microscopy in the material sciences. Mater. Charact. 60 (1), 2–13.

Reif, Wolf-Ernst, 1974. Morphologie und Ultrastruktur des Hai- "Schmelzes". Zool. Scripta 2 (5-6), 231–250.

Seow, W.K., Amaratunge, A., 1998. The effects of acid-etching on enamel from different clinical variants of amelogenesis imperfecta: an SEM study. Pediatr. Dent. 20 (1), 37–42.

Sezen, M., Sadighikia, S., 2014. 3D electron microscopy investigations of human dentin at the micro/nano-scale using focused ion beam based nanostructuring. RSC Adv. 5 (10), pp. 7196–7199.

Vennat, E. Wang, W. Genthial, R. David, B. Dursun, E., Gourrier, A. 2002. Three Dimensional Characterization of the Dentin Porous Network Using Confocal Laser Scanning Microscopy (CLSM), Poromechanics VI, p. 937-944.

Xu, Xiangyang, Xu, Shengzhou, Jin, Lianghai, Song, Enmin, 2011. Characteristic analysis of Otsu threshold and its applications. Pattern Recogn. Lett. 32 (7), 956–961.

Yoon, H.S., Newnham, R.E., 1969.. Elastic properties of fluorapatite. Am. Mineral. 54 (7–8), 1193–1197.

Zhang J. Hu, J. 2008. Image Segmentation Based on 2D Otsu Method with Histogram Analysis. In 2008 International Conference on Computer Science and Software Engineering, vol. 6, p. 105-108.